Investigation of Bite Marking Detection and Classification using Segmentation with Deep Transfer Learning Approach

Dr.M.Chandramouleeswaran[1], Dr.N.Puviarasan[2]

[1]Assistant Professor/Programmer, Department of Computer and Information Science, Annamalai University, Chidambaram, Tamilnadu, India

[2]Professor & Head, Department of Computer and Information Science, Annamalai University, Chidambaram, Tamilnadu, India.

Abstract:

Bite marking is considered an important topic in forensic investigation. The detection and classification of bite marking in the victim will be helpful to properly determine the criminals. The recent advances in computer vision (CV) and artificial intelligence (AI) models have resulted in the design of bite marking detection and classification models. At the same time, the available machine learning (ML) and deep learning (DL) models pave a way for effective bite marking detection and classification outcomes. This study investigates a new bite marking detection and classification using segmentation with deep transfer learning (BMDC-SDTL) approach. The major intention of the BMDC-SDTL technique is to determine the appropriate class labels for the bite marked images. The BMDC-SDTL technique primarily involves different stages of pre-processing. In addition, the BMDC-SDTL technique designs a new Chan-Vese segmentation approach to identify the bite marked regions. Followed by, DenseNet-169 model is employed for feature extraction process. Finally, support vector machine (SVM) and logistic regression (LOR) models are utilized as classification models. The performance validation of the BMDC-SDTL technique is performed using a dataset collected by our own. An extensive comparison study reported the better outcomes of the BMDC-SDTL technique over the other techniques.

Keywords: Deep transfer learning, Bite marking, Classification model, Image segmentation, DenseNet model

DOI: 10.24297/j.cims.2023.5.2

1. Introduction

A bite mark is a kind of evidence that might be found after a crime. But this kind of evidence needs further study and also it is controversial. Teeth are frequently employed as weapon once a victim tries to ward off an assailant (or) one person attacks another [1]. It is quite easy to record the evidence from the injury and the teeth for comparing the pattern, shape, and size. In

addition, traces of saliva deposited during biting might be recovered for acquiring DNA evidence. When the dentist is aware of different techniques to preserve and collect bitemark evidence from victims, it might be possible for them to prosecute, assist and identify violent offenders [2]. Bite mark analysis depends on the principle that 'no two mouths are the same. Thus, Bite mark is considered a valuable alternate for DNA identification and fingerprinting in forensic examination. A bite mark is a mark made by teeth alone or with other oral structures [3]. The computer vision (CV) field involves a set of challenges like localization, object detection, image classification, and segmentation [4, 5]. Amongst them, image classification is considered a major challenge. It creates the basis for another CV issue [6]. Image classification application is utilized in various fields like brake light detection, traffic control system, object identification in satellite image, medicinal imaging, machine vision, etc. [7]. Image classification is the process of assigning and categorizing labels into groups of vectors or pixels within an image based on certain rules. The categorization law is employed by using more than one textural or spectral feature [8]. Image detection using machine learning (ML) leverages the potential of algorithms for learning hidden knowledge from datasets of organized and unorganized samples. The more commonly used ML approach is deep learning (DL), where several hidden layers are utilized [9]. In comparison to the conventional CV method in earlier image processing, DL requires the knowledge of engineering of machine learning (ML) method. It does not require experts, especially machine vision area to make hand-engineered features [10].

1.1. Prior Works on Bite Marking Analysis

Rivera-Mendoza et al. [11] derived an approach to determine the variations among 3 wax test bites taken from the identical person to identify whether the initial bite has given improved quality. The study has reported that no considerable changes were obtained among the test bite count and corresponding quality. The interrater arrangement formed nearly faultless and considerable agreement. So, it is suggested to experiment with multiple bite tests in organized situations. In [12], a set of 5 bite marking samples are chosen. The bite markings are determined on the persons admitted in the hospitals and are investigated by the computer based superimposition approach by the use of Adobe Photoshop tool. The experimental results stated that the presented technique has not been excluded as having made the bite mark with suspect's dentition. Sun et al. [13] reformed the Grad-CAM technique to investigate the tooth marked tongue. Next, it is used for the localization of the middle regions in the image for predicting the pathology with no bounding boxes and accurately classifies tooth marked

tongue. After examining the visual understanding of the tooth marked issues, this work has investigated the effect of field size on the classifier outcomes.

1.2. Paper Contribution

This study develops a new bite marking detection and classification using segmentation with deep transfer learning (BMDC-SDTL) approach. The goal of the BMDC-SDTL technique is to decide the correct class labels for the bite marked images. The BMDC-SDTL technique mainly involves diverse phases of pre-processing. Moreover, the BMDC-SDTL technique designs a new Chan-Vese segmentation approach to identify the bite marked regions. Furthermore, DenseNet-169 model is employed for feature extraction process. At last, support vector machine (SVM) and logistic regression (LOR) models are utilized as classification models. The performance validation of the BMDC-SDTL technique is performed using a dataset collected by our own.

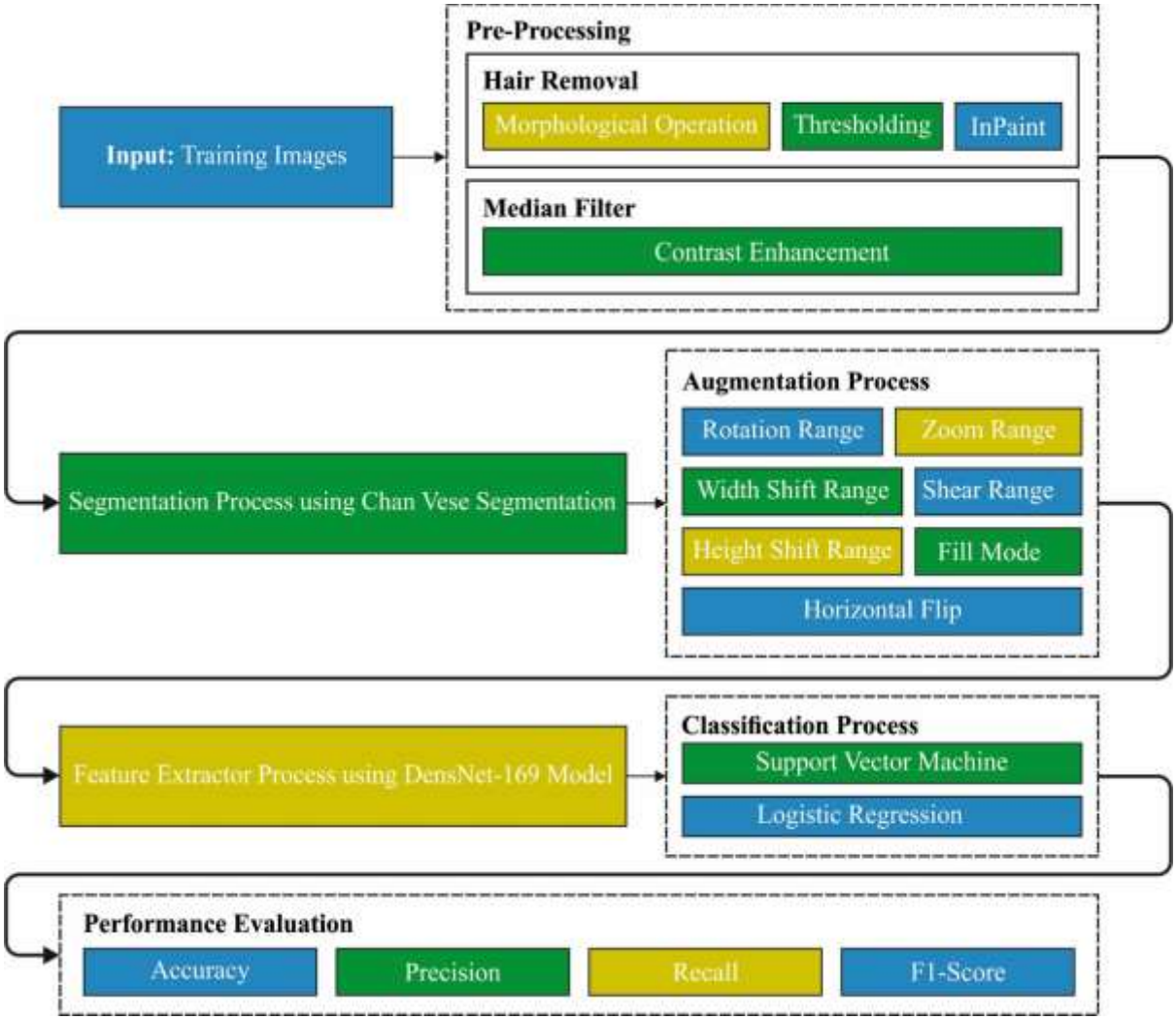

Fig. 1. Block diagram of BMDC-SDTL

2. Materials and Methods

In this section, a new BMDC-SDTL technique has been developed for the accurate detection and classification of bite marking images. The proposed BMDC-SDTL technique follows a series of subprocesses namely pre-processing, Chan-Vese segmentation, DenseNet-169 feature extraction, and classification. In this work, a set of two classifiers namely SVM and LOR models are used to determine the class labels. Fig. 1 depicts the block diagram of proposed BMDC-SDTL technique.

2.1. Stage I: Data Pre-processing

Initially, hair removal process can be done by black hat filtering. In morphology and digital image processing, top-hat transform and black-hat transform are commonly used to extract details and artefacts from the given images. The black hat transform is signified by the difference between the input and closing images. Here, it is used to eliminate the existence of minute hairs that are present in the bite marked skin region. Next, median filtering (MF) is utilized to remove the noise that presents in the bite mark images. MF method is a nonlinear process useful for reducing salt-and-pepper, or impulsive noises. Also, it is useful to preserve edge from image but reduce arbitrary noise. Next, adoptive histogram equalization (AHE) is a digital image processing method employed for improving image contrast. It differs in usual HE from the respect that adoptive approach enhances the contrast locally. It splitted the image into different blocks and calculate HE for each section. Thus, AHE computes different histograms, each equivalent to different sections of images. It enhances the local contrast and definition of edge from each distinct region of images. (Fig 3.1 Pre-processing Images)

2.2. Stage II: Determination of bite marked regions

After data pre-processing stage, the bite marked regions are identified using the Chan-Vese segmentation model [14]. Mumford and Shah introduced a Chan-Vese model that is piecewise constant approximation to the functional formulation of image segmentation. It became popular in the image processing fields primarily because of its capability to identify objects not exactly determined by a gradient. It aims to divide an input scalar image $u_0 : \Omega \to \mathbb{R}$ determined by a d-dimension image domain $\Omega \subset \mathbb{R}^d$ into two probably disconnected regions Ω_1 (foreground) and Ω_2 (background) of lower intra-region variance and divided by a smooth closed contour $C(\Omega = \Omega_1 \cup \Omega_2 \cup C)$.

$$E_{CV}(C, c_1, c_2) = \mu|C| + \lambda_1 \int_{\Omega_1} (u_0(x) - c_1)^2 dx + \lambda_2 \int_{\Omega_2} (u_0(x) - c_2)^2 dx \quad (1)$$

Whereas c_1 and c_2 denotes the unknown average intensity levels inside Ω_1 and Ω_2, correspondingly, and μ, λ_1, and λ_2 indicates positive, user-determined weight. Herein, the first term is the regularization term and the other as fidelity term. The optimum segmentation C, c_1, c_2) corresponding to global minimum of (1). (Fig.3.2 Segmentation Images)

2.3. Data augmentation

For increasing the size of training and testing dataset, data augmentation process take place as follows. rotation_range = 20, zoom_range = 0.15, width_shift_range = 0.2, height_shift_range = 0.2, shear_range = 0.15, horizontal_flip = True, and fill_mode = "nearest". (Fig.4 Augmented Images)

2.4. Stage III: DenseNet-169 based Feature Extraction

During feature extraction process, the DenseNet-169 model is employed. DenseNet is a new architecture of convolution deep learning. The concept is to construct a deep framework that has connections among all the convolutional layers to all the layers within a similar dense block in a feed-forward manner. Different from the ResNet [15], the connection of DenseNet is in feature-level rather than weight-level. The parameter of all the layers would be trained, and the resulting feature-map would be concatenated together as the input. Likewise, the weight might be very effective, and the gradient won' t be disappeared. For DenseNet, feature is passed to each succeeding layer in all the dense blocks. Thus, the l − th layer get the feature-map from each preceding layer as input:

$$\mathrm{x_l} = \mathrm{H}([\mathrm{x_0}: \mathrm{x_1}: \ldots : \mathrm{x_{l-1}}]) \quad (2)$$

Whereas, $[\mathrm{x_0}: \mathrm{x_1}: \ldots : \mathrm{x_{l-1}}]$ represent the concatenation of feature-map generated in layers $0, \ldots, l-1$. Generally, there are different dense blocks, one classification layer and three transition layers in DenseNet. Initially, DenseNet-169 [15], a convolution of 7×7 kernel using stride 2×2 is utilized. However, in the similar location of DenseNet-, then implement a convolutional process alongside the dimension for getting the fundamental feature-map. The convolution has 5×5 kernel 1, without pooling function. There are four dense blocks, also the amount of layers in all the dense blocks is distinct in DenseNet121, DenseNet169. The concatenation function in Eq. (2) rapidly increasing the input size as the amount of layer increases. There is an average pooling layer in the transition layer. Thus, down-sampling the size

of feature-maps is needed that is performed in the transition layer. In the classifier layer of the DenseNet architecture, there is a FC layer and a global average pooling layer. Fig. 2 demonstrates the layers in DenseNet-169 Model.

Layers	Output Size	DenseNet-121	DenseNet-169	DenseNet-201	DenseNet-264
Convolution	112 × 112	7 × 7 conv, stride 2			
Pooling	56 × 56	3 × 3 max pool, stride 2			
Dense Block (1)	56 × 56	[1 × 1 conv, 3 × 3 conv] × 6	[1 × 1 conv, 3 × 3 conv] × 6	[1 × 1 conv, 3 × 3 conv] × 6	[1 × 1 conv, 3 × 3 conv] × 6
Transition Layer (1)	56 × 56	1 × 1 conv			
	28 × 28	2 × 2 average pool, stride 2			
Dense Block (2)	28 × 28	[1 × 1 conv, 3 × 3 conv] × 12	[1 × 1 conv, 3 × 3 conv] × 12	[1 × 1 conv, 3 × 3 conv] × 12	[1 × 1 conv, 3 × 3 conv] × 12
Transition Layer (2)	28 × 28	1 × 1 conv			
	14 × 14	2 × 2 average pool, stride 2			
Dense Block (3)	14 × 14	[1 × 1 conv, 3 × 3 conv] × 24	[1 × 1 conv, 3 × 3 conv] × 32	[1 × 1 conv, 3 × 3 conv] × 48	[1 × 1 conv, 3 × 3 conv] × 64
Transition Layer (3)	14 × 14	1 × 1 conv			
	7 × 7	2 × 2 average pool, stride 2			
Dense Block (4)	7 × 7	[1 × 1 conv, 3 × 3 conv] × 16	[1 × 1 conv, 3 × 3 conv] × 32	[1 × 1 conv, 3 × 3 conv] × 32	[1 × 1 conv, 3 × 3 conv] × 48
Classification Layer	1 × 1	7 × 7 global average pool			
		1000D fully-connected, softmax			

Fig. 2. Layers in DenseNet-169 Model

2.5. Stage IV: Bite Marking Classification

At the final stage, the SVM and LOR models are utilized for bite marking classification [16, 17]. SVM approach was initially proposed for linear binary classification. The approach constructs a hyperplane to split positive and negative samples with the margin. But the samples are not linearly separable and this hyperplane doesn' t occur. It might lead to poor performance. Consequently, the original SVM approach is expanded for non-linear classification by using kernel function. Assume a training set contains N samples $\{x_k, y_k\}_{k=1}^{N}$, whereas $x_k \in R^n$ denotes a feature or input vector and $y_k \in \{-1, +1\}$ indicates the response or class label. The training process of the SVM is arithmetically expressed as follows

$$J_p(w, e) = \frac{1}{2} w^T w + C \frac{1}{2} \sum_{k=1}^{N} e_k^2, \quad (3)$$

subject to

$$y_k(w^T \phi(x_k) + b) \geq 1 - e_k, k = 1, \ldots, N, e_k \geq 0, \quad (4)$$

where the results $w \in R^n$ and $b \in R$ determine the classification hyperplane; the result e denotes the vector of slack variable presented to manage the case data could not be divided without error; C indicates the penalty constant decides how much weight must be put on classification

error, and $\phi(x)$ indicates the non-linear mapping from the input space to a high-dimension space.

LOR derives from the supervised classifier technique. This technique was utilized for classifying individuals in categories dependent upon logistic function. For understanding the mathematical version of explanation, it starts with easy linear regression equation

$$y = b0 + b1 * x \quad (5)$$

Therefore, the sigmoid function was implemented on it, and it can be provided as the equation:

$$p = \frac{1}{1 + e^{-y}} \quad (6)$$

At this point, the value of y is computed by substituting equation (5) on equation (6); LOR equation is obtained as follows:

$$\ln\left(\frac{p}{1-p}\right) = b0 + b1 * x \quad (7)$$

Or logit $(S) = b0 + b1M1 + b2M2 + b3M3 \ldots bkMk$ ...whereas, S refer the probability of presence of the interest features. $M1, M2, M3 \ldots \ldots Mk$ are the predictor value $b0, b1, b2, b3 \ldots \ldots bk$ are the intercept of models.

3. Performance Validation

In this section, the bite marking classification outcomes of the proposed model is validated. For experimental purposes, we have collected our own dataset comprising 12 classes with 2 images under each class. In order to increase the size of the dataset, data augmentation is carried out and the number of images under every class becomes 32. A set of sample images are shown in Fig. 3. Therefore, the dataset holds a total of 384 images. Fig. 4 demonstrates the sample set of augmented images.

Fig. 3. Sample Images

Fig. 3.1 Pre-processing Images

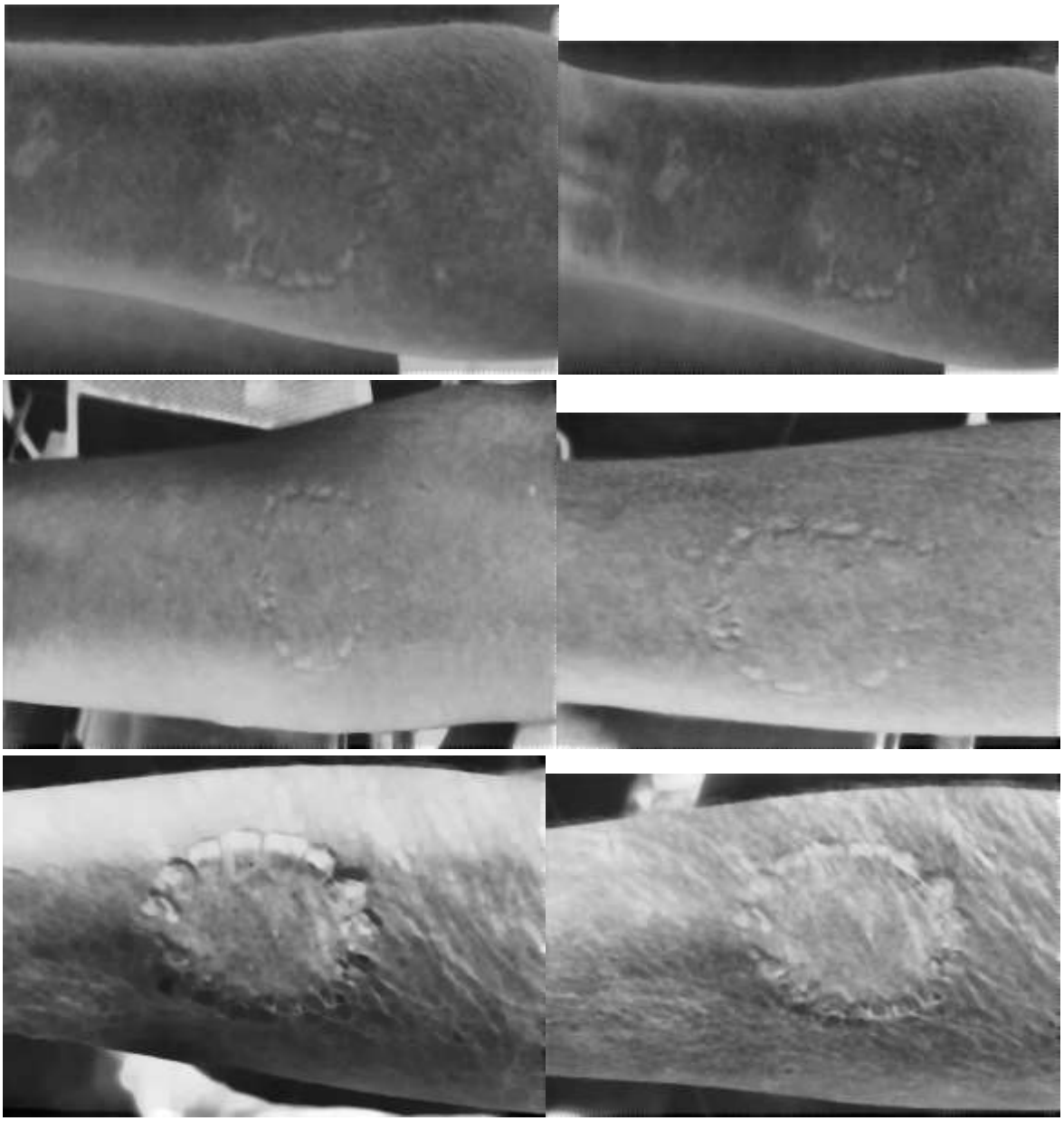

Fig. 3.2 Segmentation Images

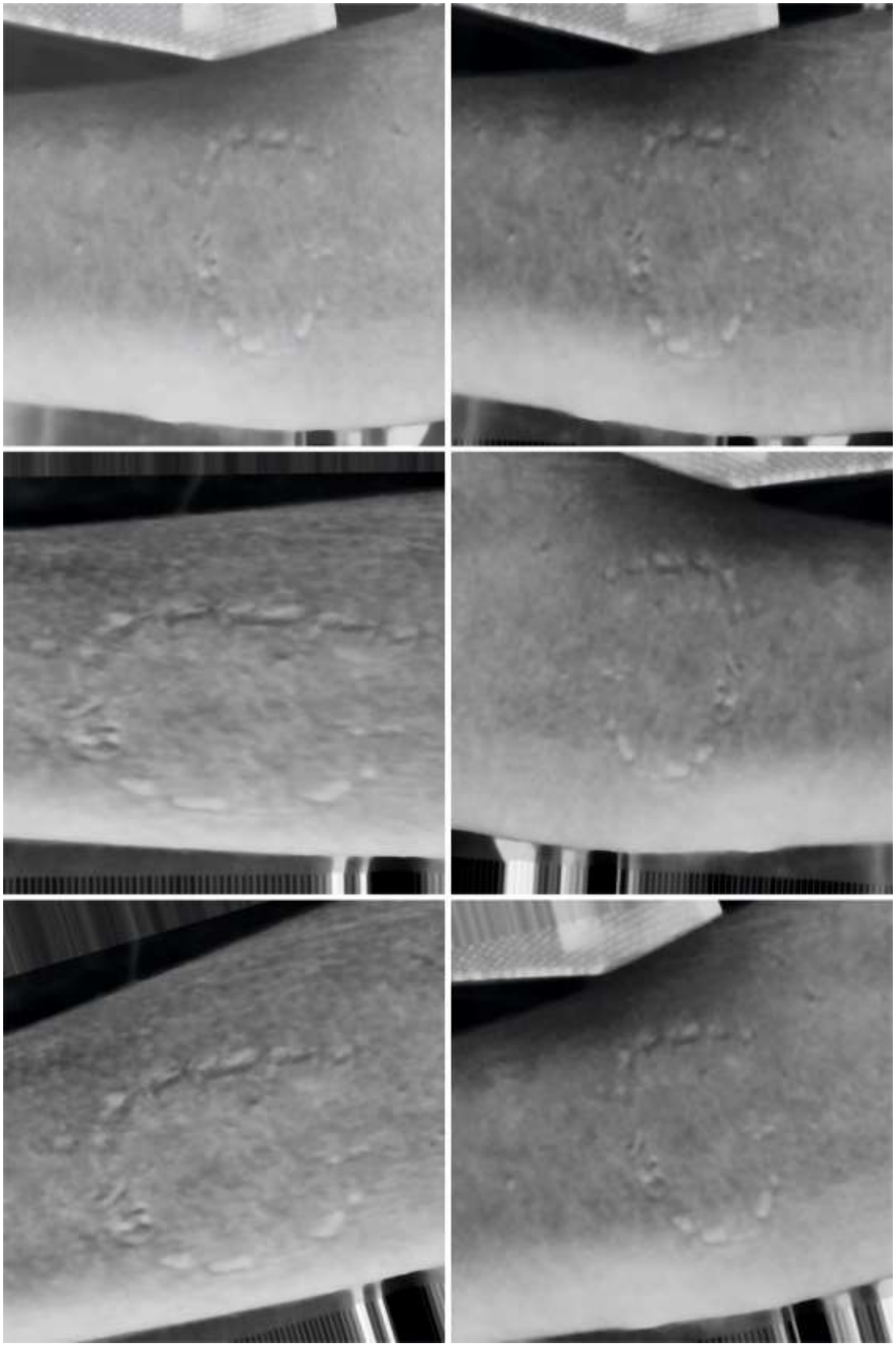

Fig. 4. Augmented Images

The confusion matrix produced by the DenseNet-SVM model on the training phase is offered in Fig. 5. The figures indicated that the DenseNet-SVM model has recognized 17 images into class 1, 24 images into class 2, 16 images into class 3, 17 images into class 4, 24 images into class 5, 16 images into class 6, 22 images into class 7, 17 images into class 8, 19 images into class 9, 23 images into class 10, 14 images into class 11, and 21 images into class 12.

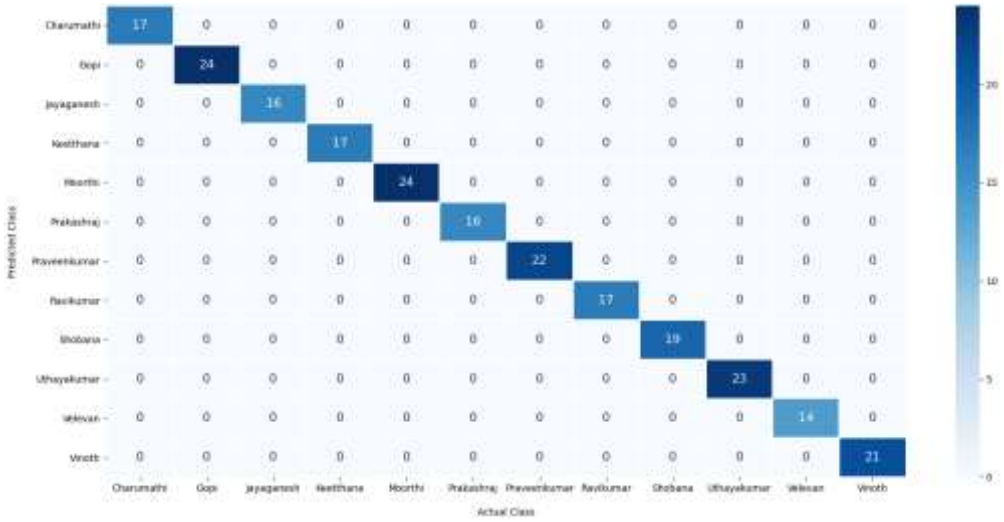

Fig. 5. Confusion matrix of DenseNet-SVM (Training Phase)

The confusion matrix produced by the DenseNet-SVM technique in the testing phase is shown in Fig. 6. The figures showed that the DenseNet-SVM approach has recognized 15 images into class 1, 8 images into class 2, 12 images into class 3, 15 images into class 4, 8 images into class 5, 16 images into class 6, 10 images into class 7, 13 images into class 8, 13 images into class 9, 9 images into class 10, 17 images into class 11, and 11 images into class 12.

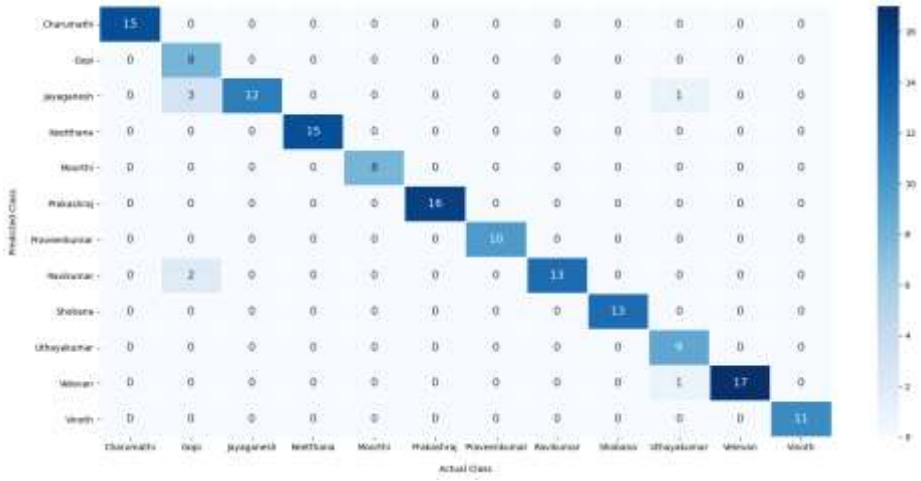

Fig. 6. Confusion matrix of DenseNet-SVM (Testing Phase)

The confusion matrix produced by the DenseNet-LOR technique on the training phase is shown in Fig. 7. The figures showed that the DenseNet-LOR approach has recognized 17 images into class 1, 24 images into class 2, 16 images into class 3, 17 images into class 4, 24 images into class 5, 16 images into class 6, 22 images into class 7, 17 images into class 8, 19 images into class 9, 23 images into class 10, 14 images into class 11, and 21 images into class 12.

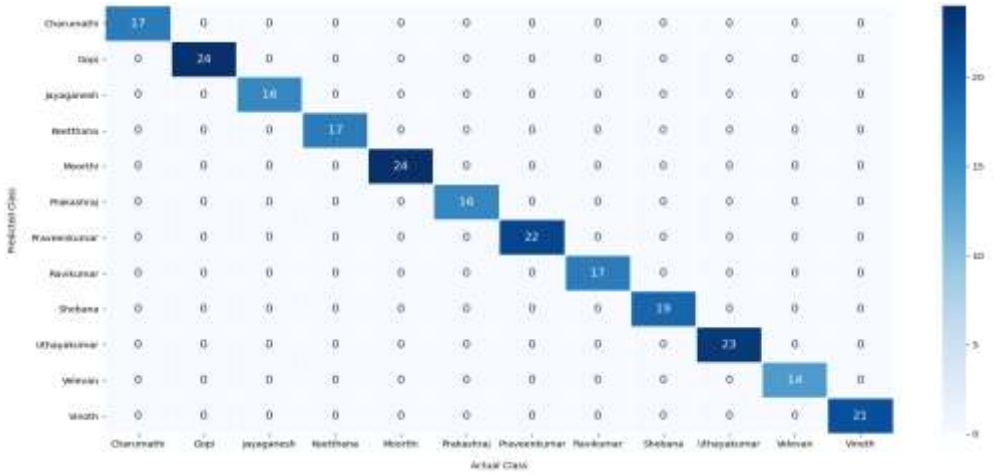

Fig. 7. Confusion matrix of DenseNet-LOR (Training Phase)

The confusion matrix produced by the DenseNet-LOR technique on the testing phase is shown in Fig. 8. The figures exposed that the DenseNet-LOR algorithm has recognized 17 images into class 1, 15 images into class 2, 8 images into class 3, 15 images into class 4, 8 images into class 5, 16 images into class 6, 10 images into class 7, 15 images into class 8, 13 images into class 9, 9 images into class 10, 18 images into class 11, and 10 images into class 12.

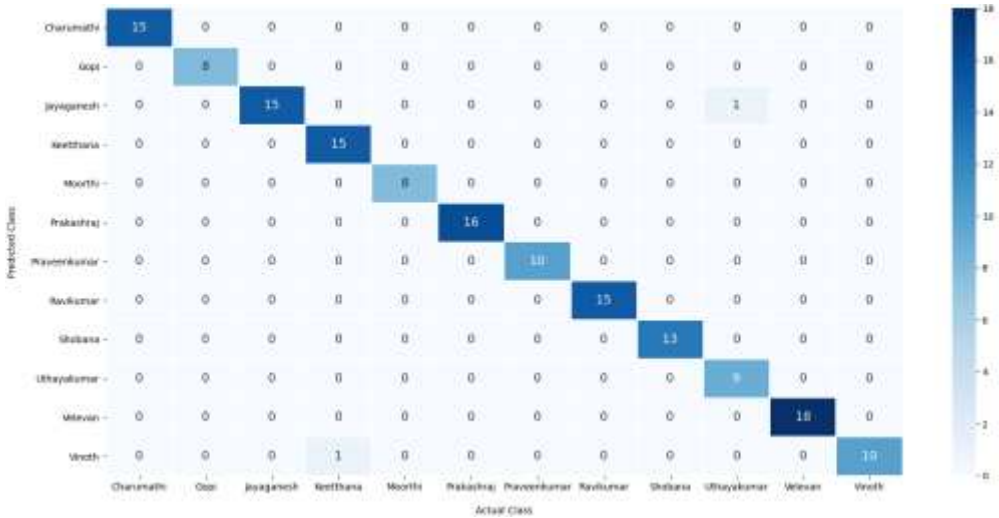

Fig. 8. Confusion matrix of DenseNet-LOR (Testing Phase)

Fig. 9 validates the accuracy assessment of the DenseNet-SVM approach under training and testing dataset. The results described that the DenseNet-SVM model has the aptitude of gaining improved values of training and validation accuracies. It can be visible that the validation accuracy values are somewhat higher than training accuracy.

A brief training and validation loss offered by the DenseNet-SVM technique are reported in Fig. 10 under training and testing dataset. The results revealed that the DenseNet-SVM model has accomplished minimum values of training and validation losses.

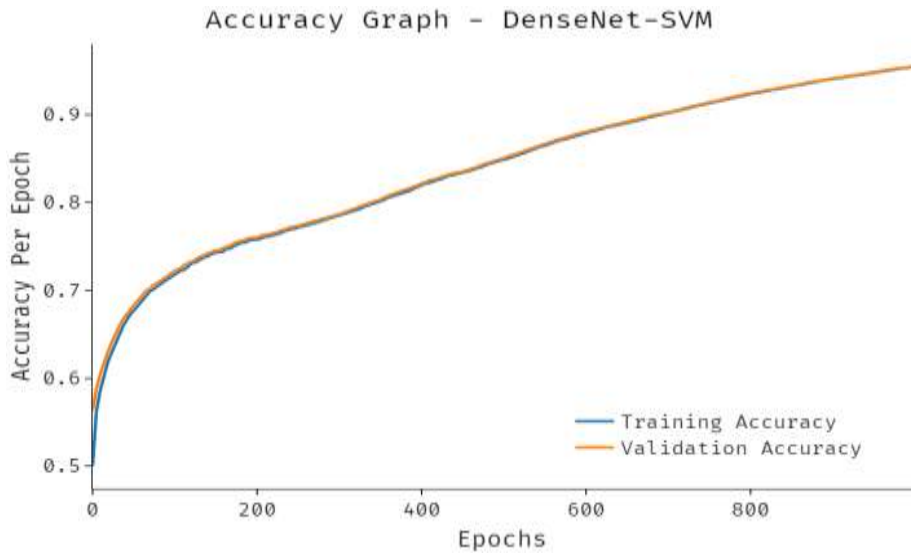

Fig. 9. Accuracy Graph of DenseNet-SVM technique

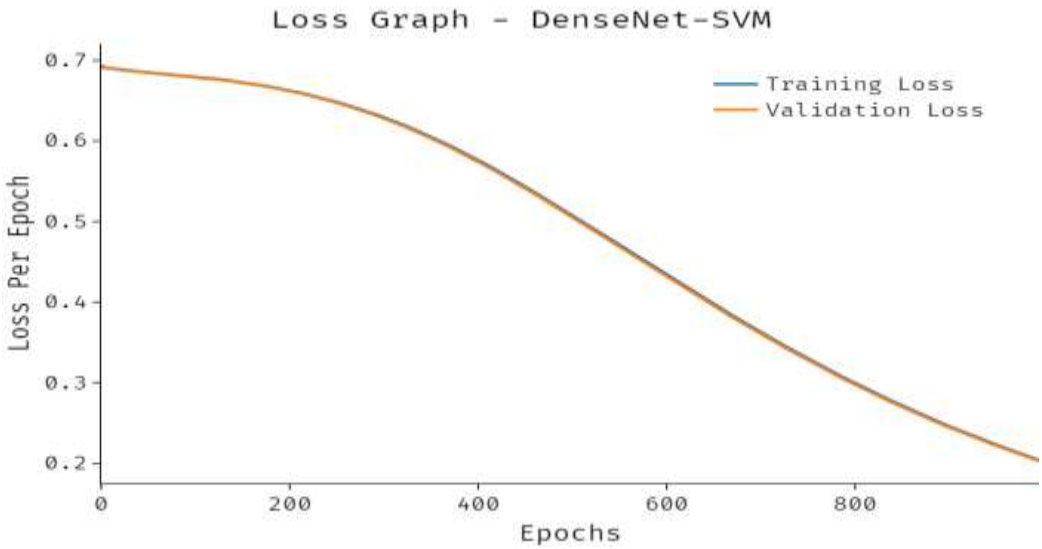

Fig. 10. Loss Graph of DenseNet-SVM technique

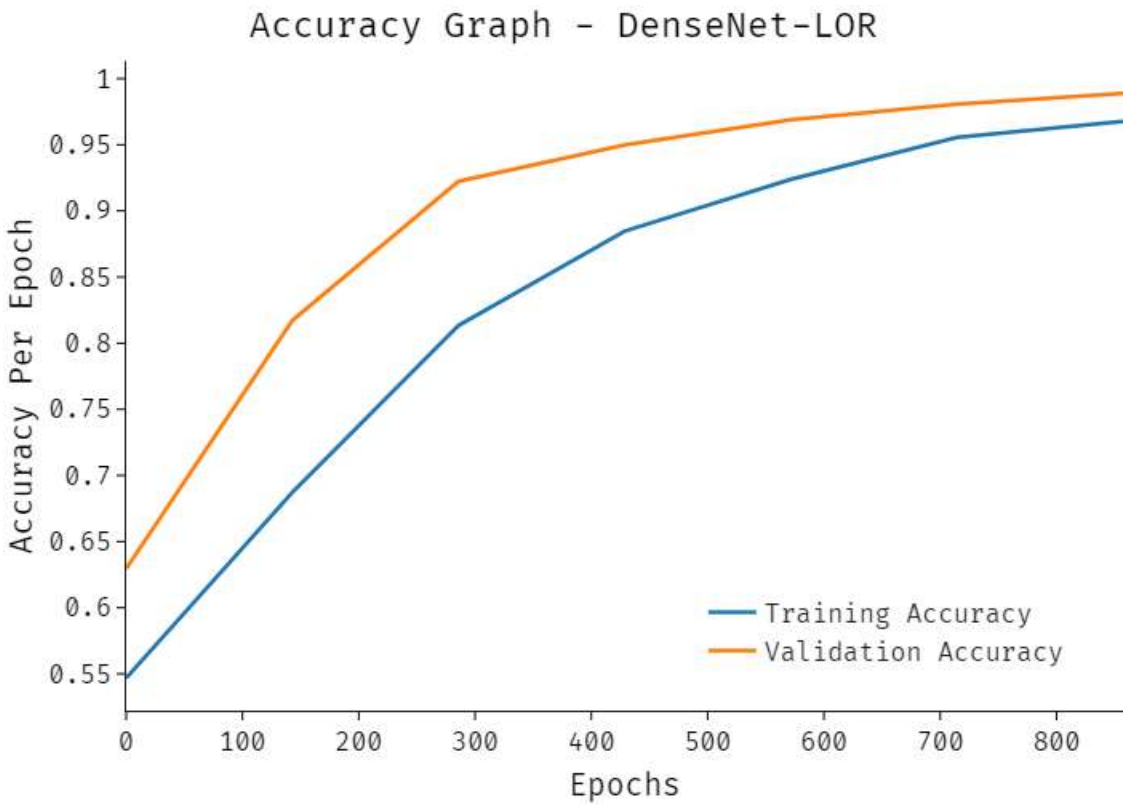

Fig. 11. Accuracy Graph of DenseNet-LOR technique

Fig. 11 validates the accuracy assessment of the DenseNet-LOR system under training and testing dataset. The outcomes described that the DenseNet-LOR approach has the aptitude of gaining improved values of training and validation accuracies. It is visible that the validation accuracy values are slightly higher than training accuracy.

A detailed training and validation loss offered by the DenseNet-LOR algorithm is reported in Fig. 12 under training and testing dataset. The results revealed that the DenseNet-LOR system has accomplished minimal values of training and validation losses.

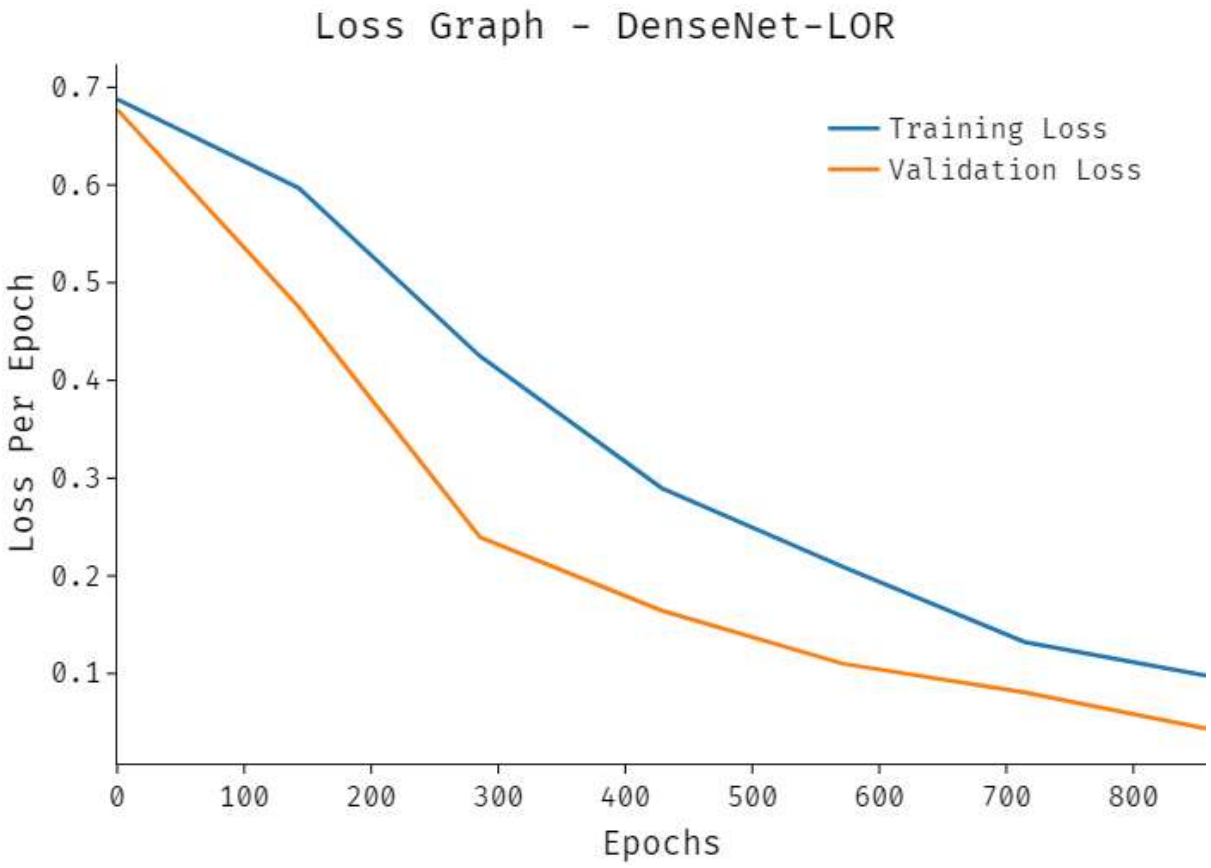

Fig. 12. Loss Graph of DenseNet-LOR technique

Table 1 and Fig. 13 reports the overall bite marking classification outcomes of the DenseNet-SVM and DenseNet-LOR models. From the experimental values, it is noticed that the DenseNet-SVM model has accomplished $accu_y$ of 95.45%, $prec_n$ of 95.28%, $reca_l$ of 96.34%, and $F1_{score}$ of 95.16%. Besides, the DenseNet-LOR model has obtained $accu_y$ of 98.70%, $prec_n$ of 98.65%, $reca_l$ of 98.72%, and $F1_{score}$ of 98.63%.

Table 1 Result analysis of BMDC-SDTL with different measures

Methods	Accuracy (%)	Precision (%)	Recall (%)	F1-Score (%)
DenseNet-SVM	95.45	95.28	96.34	95.16
DenseNet-LOR	98.70	98.65	98.72	98.63

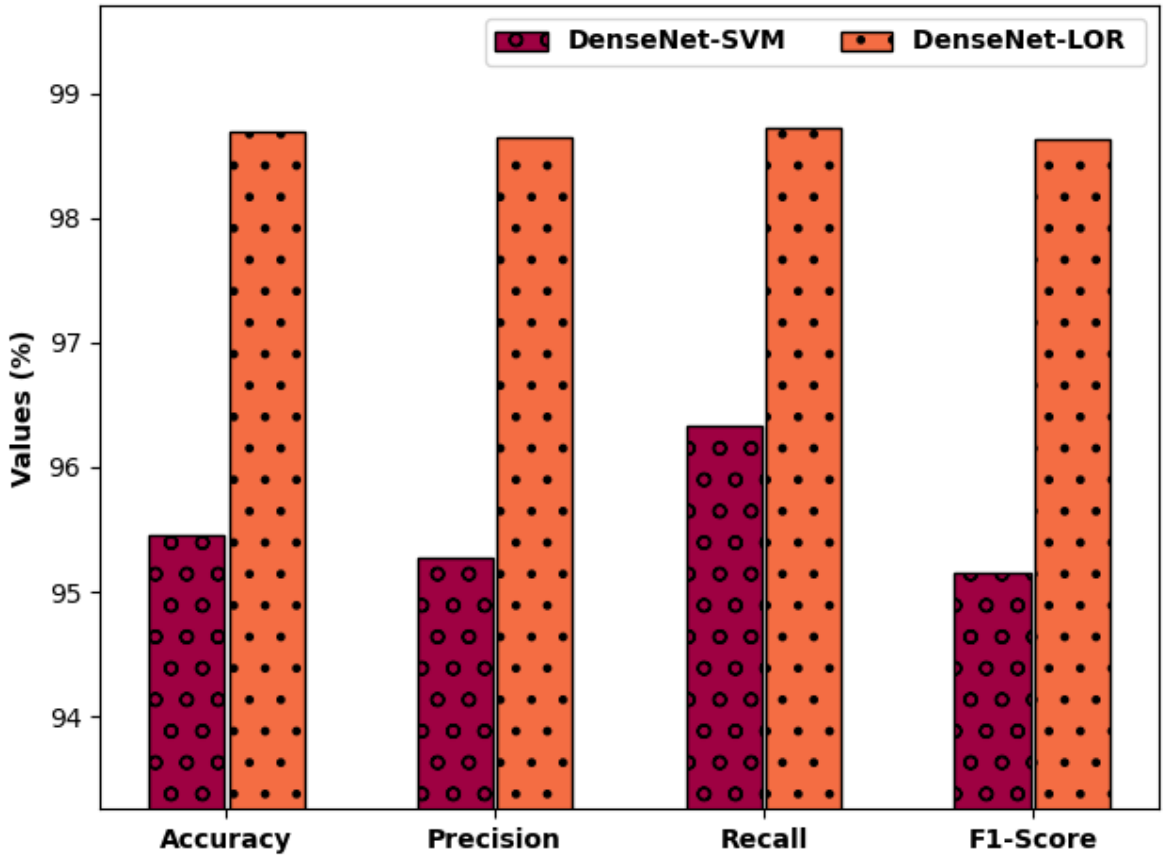

Fig. 13. Result analysis of BMDC-SDTL with different measures

Table 1 reports the comparative classification outcomes of the proposed model with existing techniques. The results indicated that the DenseNet-LOR model has resulted in maximum classification performance.

A brief comparative study of the proposed model with existing models in terms of $prec_n$ is illustrated in Fig. 14. The experimental results indicated that the CNN Layer-3 and CNN Layer-6 models have resulted to lower $prec_n$ of 70.40% and 72.50% respectively. At the same time, the CNN Layer-4 and CNN Layer-5 models have offered slightly improved $prec_n$ values of 77% and 75.90%. At the same time, the DenseNet-SVM model has resulted in reasonable performance with $prec_n$ of 95.28%. However, the DenseNet-LOR has accomplished maximum $prec_n$ of 98.65%.

Table 2 Comparative analysis of BMDC-SDTL with recent approaches

Methods	Precision	Recall	Accuracy	F-Score
CNN Layer-3	70.40	62.10	71.30	66.00

CNN Layer-4	77.00	56.10	73.60	65.00
CNN Layer-5	75.90	78.10	78.60	77.00
CNN Layer-6	72.50	67.70	72.10	70.00
DenseNet-SVM	95.28	96.34	95.45	95.16
DenseNet-LOR	98.65	98.72	98.70	98.63

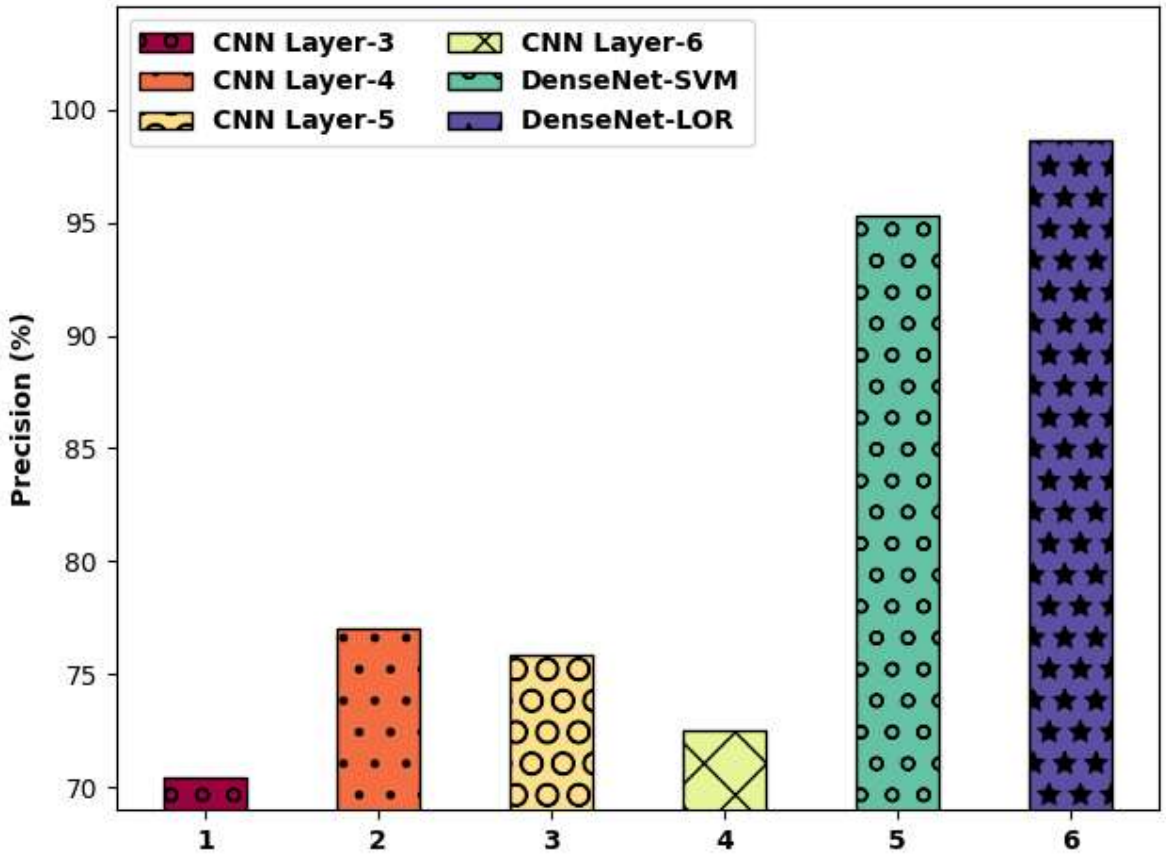

Fig. 14. $Prec_n$ analysis of BMDC-SDTL with recent approaches

A detailed comparison study of the proposed method with existing models in terms of $reca_l$ is illustrated in Fig. 15. The experimental outcomes exposed that the CNN Layer-4 and CNN Layer-3 models have resulted to reduce $reca_l$ of 56.10% and 62.10% correspondingly. Also, the CNN Layer-6 and CNN Layer-5 models have offered somewhat higher $reca_l$ values of 67.70% and 78.10%. Afterward, the DenseNet-SVM technique has resulted in reasonable performance with $reca_l$ of 96.34%. Finally, the DenseNet-LOR approach has accomplished maximal $reca_l$ of 98.72%.

A brief comparative study of the proposed technique with existing models with respect to acc_y is illustrated in Fig. 16. The experimental results revealed that the CNN Layer-3 and CNN Layer-6 models have resulted in minimum acc_y of 71.30% and 72.10% correspondingly. Along with that, the CNN Layer-4 and CNN Layer-5 models have offered somewhat enhanced acc_y values of 73.60% and 78.0%. Likewise, the DenseNet-SVM system has resulted in reasonable performance with acc_y of 95.45%. At last, the DenseNet-LOR methodology has accomplished higher acc_y of 98.70%.

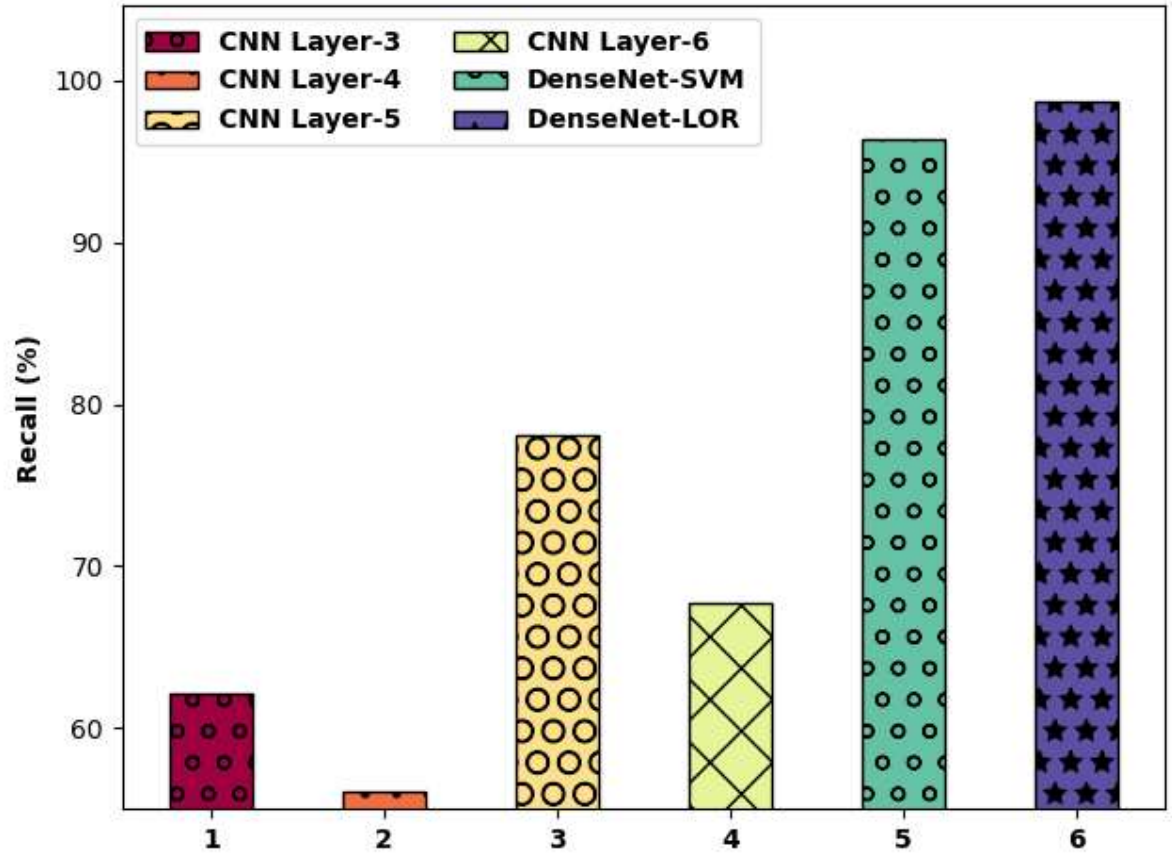

Fig. 15. $Reca_l$ analysis of BMDC-SDTL with recent approaches

A detailed comparison study of the proposed model with existing models in terms of F_{score} is illustrated in Fig. 17. The experimental results indicated that the CNN Layer-3 and CNN Layer-4 approaches have resulted in lesser F_{score} of 66% and 65% correspondingly. Followed by, the CNN Layer-6 and CNN Layer-5 techniques have offered enhanced F_{score} values of 70% and 77%. In line with, the DenseNet-SVM methodology has resulted in reasonable performance with F_{score} of 95.16%. Eventually, the DenseNet-LOR method has accomplished increased F_{score} of 98.63%.

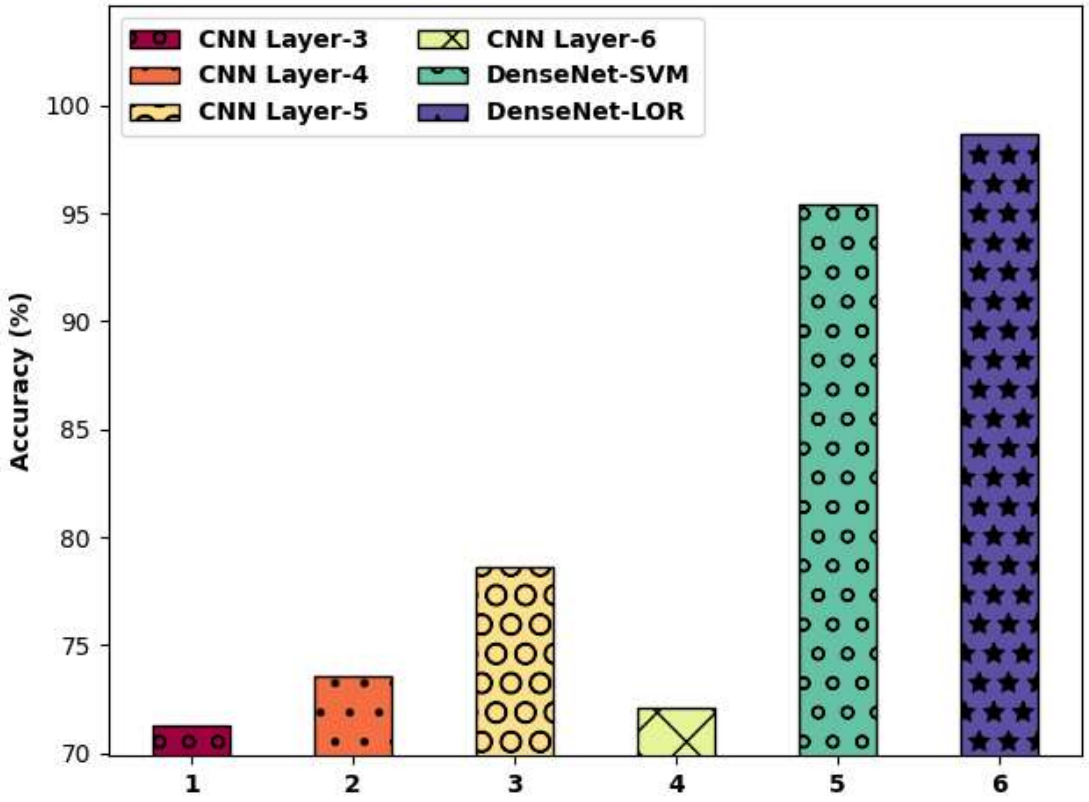

Fig. 16. Acc_y analysis of BMDC-SDTL with recent approaches

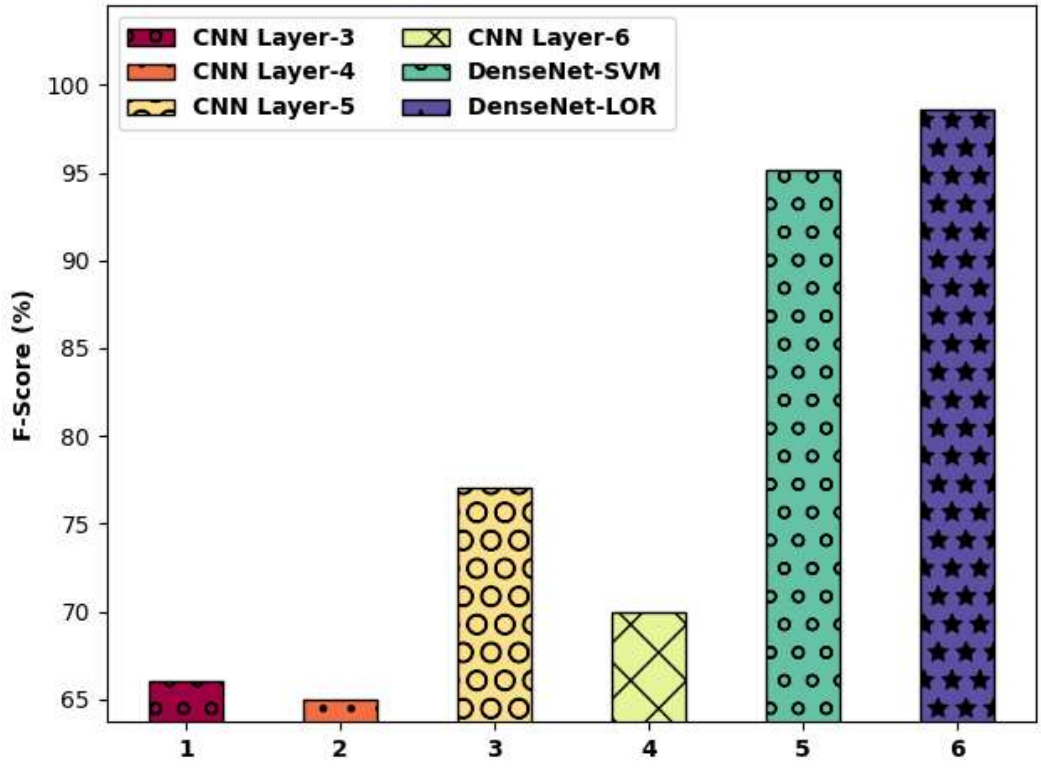

Fig. 17. F_{score} analysis of BMDC-SDTL with recent approaches

After examining the above mentioned tables and figures, it is evident that the DenseNet-LOR model has the ability to obtain maximum bite mark classification performance.

4. Conclusion

In this study, a new BMDC-SDTL technique has been developed for the accurate detection and classification of bite marking images. The proposed BMDC-SDTL technique follows a series of subprocesses namely pre-processing, Chan-Vese segmentation, DenseNet-169 feature extraction, and classification. In this work, a set of two classifiers namely SVM and LOR models are used to determine the class labels. The performance validation of the BMDC-SDTL technique is performed using a dataset collected by our own. Extensive comparison studies reported better outcomes of the BMDC-SDTL technique over the other techniques. Thus, the BMDC-SDTL technique can appear as an effectual tool for bite marking detection and classification. In future, the classification outcomes of the BMDC-SDTL technique can be boosted by the design of hybrid DL models.

References

1. Chinni SS, Al-Ibrahim A, Forgie AH (2013) A simple safe, reliable and reproducible mechanism for producing experimental bite marks. J Forensic Odontostomatol 31(1):22–29.
2. Franco A, Willems G, Souza P, Coucke W, Thevissen P (2017) Uniqueness of the anterior dentition three-dimensionally assessed for forensic bitemark analysis. J Forensic Legal Med 46:58–65.
3. Rivera-Mendoza F, Martín-de-Las-Heras S, Navarro-Cáceres P, Fonseca GM (2017) Bite mark analysis in foodstuffs and inanimate objects and the underlying proofs for validity and judicial acceptance. J Forensic Sci
4. Saks MJ, Albright T, Bohan TL et al (2016) Forensic bitemark identification: weak foundations, exaggerated claims. J Law Biosci 3:538–575.
5. Dama, N., Forgie, A., Mânica, S. and Revie, G., 2020. Exploring the degrees of distortion in simulated human bite marks. *International journal of legal medicine*, *134*(3), pp.1043-1049.
6. Mikołajczyk, A. and Grochowski, M., 2018, May. Data augmentation for improving deep learning in image classification problem. In *2018 international interdisciplinary PhD workshop (IIPhDW)* (pp. 117-122). IEEE.

7. Wang, P., Fan, E. and Wang, P., 2021. Comparative analysis of image classification algorithms based on traditional machine learning and deep learning. *Pattern Recognition Letters*, *141*, pp.61-67.
8. Korot, E., Guan, Z., Ferraz, D., Wagner, S.K., Zhang, G., Liu, X., Faes, L., Pontikos, N., Finlayson, S.G., Khalid, H. and Moraes, G., 2021. Code-free deep learning for multi-modality medical image classification. *Nature Machine Intelligence*, *3*(4), pp.288-298.
9. Jena, B., Saxena, S., Nayak, G.K., Saba, L., Sharma, N. and Suri, J.S., 2021. Artificial intelligence-based hybrid deep learning models for image classification: The first narrative review. *Computers in Biology and Medicine*, *137*, p.104803.
10. Haq, M.A., Rahaman, G., Baral, P. and Ghosh, A., 2021. Deep learning based supervised image classification using UAV images for forest areas classification. *Journal of the Indian Society of Remote Sensing*, *49*(3), pp.601-606.
11. Rivera-Mendoza, F., Martín-de-las-Heras, S., Navarro-Cáceres, P. and Fonseca, G.M., 2018. Selection of test bites records as part of a forensic bite mark analysis protocol. Egyptian Journal of Forensic Sciences, 8(1), pp.1-8.
12. Chintala, L., Manjula, M., Goyal, S., Chaitanya, V., Hussain, M.K.A. and Chaitanya, Y.C., 2018. Human bite marks–a computer-based analysis using adobe photoshop. Journal of Indian Academy of Oral Medicine and Radiology, 30(1), p.58.
13. Sun, Y., Dai, S., Li, J., Zhang, Y. and Li, X., 2019. Tooth-marked tongue recognition using gradient-weighted class activation maps. Future Internet, 11(2), p.45.
14. Castilla, C., Maška, M., Sorokin, D.V., Meijering, E. and Ortiz-de-Solorzano, C., 2018, April. Segmentation of actin-stained 3D fluorescent cells with filopodial protrusions using convolutional neural networks. In *2018 IEEE 15th International Symposium on Biomedical Imaging (ISBI 2018)* (pp. 413-417). IEEE.
15. Zeng, M. and Xiao, N., 2019. Effective combination of DenseNet and BiLSTM for keyword spotting. *IEEE Access*, *7*, pp.10767-10775.
16. Shah, K., Patel, H., Sanghvi, D. and Shah, M., 2020. A comparative analysis of logistic regression, random forest and KNN models for the text classification. *Augmented Human Research*, *5*(1), pp.1-16.
17. Dinh, T.V., Nguyen, H., Tran, X.L. and Hoang, N.D., 2021. Predicting rainfall-induced soil erosion based on a hybridization of adaptive differential evolution and support vector machine classification. *Mathematical Problems in Engineering*, *2021*